PERMAFROST AND PERIGLACIAL PROCESSES
Permafrost Periglac. Process. **11**: 315–326 (2000)

Surface Geometry, Thickness Changes and Flow Fields on Creeping Mountain Permafrost: Automatic Extraction by Digital Image Analysis

A. Kääb and M. Vollmer*

Department of Geography, University of Zurich, Winterthurerstrasse 190, CH-8057 Zurich, Switzerland

ABSTRACT

Aerial photogrammetry is an established tool for area-wide mapping and monitoring of permafrost geometry, thickness changes and surface creep. This study applies commercial software for the automatic generation of elevation models from digital imagery and presents a newly developed tool for digital measurement of surface displacements from repeated orthophotos. The accuracy and quality of automatically-derived geometry and velocity data are compared to conventionally-derived elevation and velocity data from the Muragl rock glacier in the Swiss Alps. The analysis reveals that for thickness changes and velocities digital photogrammetry provides at least the same accuracy as the reference data. Under unfavourable terrain and image conditions, such as steep slopes, shadows or snow cover, the reliability of the automatically-derived data is significantly lower than the operator-measured ones. Copyright © 2000 John Wiley & Sons, Ltd.

RÉSUMÉ

La photogrammétrie aérienne est un outil reconnu pour cartographier et suivre l'évolution du pergélisol, et spécialement pour déterminer les changements d'épaisseur et la vitesse du creep en surface. La présente étude s'intéresse aux programmes automatiques mesurant l'altitude à partir d'images digitales; elle présente ce nouvel outil pour connaître les déplacements de surface en comparant des orthophotos prises à différents moments. La précision et la qualité des données automatiquement obtenues sont comparées avcc les mesures d'altitude et de vitesse obtenues de la manière habituelle pour le glacier rocheux Muragl dans les Alpes suisses. L'analyse révèle que la photogrammétrie digitale donne au moins la même précision que les données de référence. Sous des conditions de terrain et d'image défavorables telles que des pentes fortes, des zones à l'ombre ou sous couverture neigeuse, la fiabilité des données obtenues automatiquement est significativement inférieure à celles obtenues par un opérateur. Copyright © 2000 John Wiley & Sons, Ltd.

KEY WORDS: Creep; digital photogrammetry; elevation model; permafrost; rock glacier; Swiss Alps

INTRODUCTION

Creeping mountain permafrost, best expressed as the so-called rock glaciers, is basically defined by its material properties and thermal conditions, and by its deformation. Thus, knowledge about three-dimensional surface velocities contributes decisively towards detecting and understanding the dynamic processes involved in space and time (e.g. Haeberli *et al.*, 1998; Berthling *et al.*, 1998; Konrad *et al.*, 1999; Frauenfelder and Kääb, 2000). Ice/rock mixtures creep with characteristic surface velocities of

* Correspondence to: Dr. A. Kääb, Department of Geography, University of Zurich, Winterthurerstrasse 190, 8057 Zurich, Switzerland. E-mail: kaeaeb@geo.unizh.ch

Received 18 May 2000
Revised 28 August 2000
Accepted 1 September 2000

centimetres, decimetres and sometimes up to a few metres per year. Their thermal inertia with low rates of freezing and thawing at the permafrost table and the permafrost base stabilize boundary conditions, so that the geometry and flow regime of perennially frozen ground on mountain slopes change slowly with time. Such climate-induced evolution of surface geometry is markedly overlain by three-dimensional straining and mass advection (Kääb *et al*., 1997; 1998). The implications from measured three-dimensional surface velocity fields cover various thermo-mechanic processes such as creep, frost heave and thaw settlement, or material properties. Further processing and modelling allow for enhanced analysis: spatial derivatives show basic characteristics of the creep regime, i.e. extending and compressive flow (Kääb *et al*., 1997); the spatial age structure and the general age can be estimated from stream-line interpolation (Kääb *et al*., 1998; Haeberli *et al*., 1999); modelling work based on the kinematic boundary condition at the surface and its simplifications help quantify the processes involved in the spatio-temporal evolution of surface geometry (Kääb *et al*., 1998; Kaufmann, 1998).

Optimal investigation of permafrost creep requires: (1) area-wide information on kinetics to account for 3-D effects, (2) in view of the low deformation rates, the application of precise high-resolution techniques, and (3) long-term monitoring for documenting slow temporal changes at a sufficient level of accuracy. As demonstrated by numerous earlier studies, photogrammetry based on repeated aerial photography represents a powerful remote-sensing tool to measure such slow geometrical changes of alpine permafrost surfaces:

(a) manual or analogue, point-by-point, measurements (Messerli and Zurbuchen, 1968; Barsch and Hell, 1975; Gorbunov and Titkov, 1992)
(b) direct analogue comparison of repeated images (Haeberli *et al*., 1979)
(c) computer-based, point-by-point, measurements (Kaufmann, 1998; Krummenacher *et al*., 1998)
(d) computer-based simultaneous comparison (Haeberli and Schmid, 1988; Kääb *et al*., 1997; 1998)
(e) fully digital deformation measurement (Ladstädter, 1999; this study).

The choice of method used mostly depends on the available photography and photogrammetric equipment.

In this study, we present a fully digital chain of image processing and analysing techniques for the automatic determination of surface geometry, permafrost thickness changes with time and surface displacements on creeping permafrost from repeated aerial photography.

TEST SITE AND REFERENCE DATA

The test site chosen for the digital photogrammetric investigations was the rock glacier in the Muragl valley (Val Muragl) in the Upper Engadine, Swiss Alps (approx. 9°55′30″ E, 46°30′15″ N). The rock glacier has an area of approx. 0.12 km^2 and an altitudinal extent of approx. 2500–2850 m ASL (cf. Figure 1). The highest surface slopes, of 25°, can be found in the upper zone underneath the terminating rock walls and in the middle part at an elevation of approx. 2600 m ASL. The typical diameter of the surface debris, an important parameter for optical contrast and thus for the applicability of photogrammetric methods, is 0.5–1.5 m. The rock glacier shows a complex topography with a number of transverse and longitudinal ridges and furrows.

The Val Muragl rock glacier has been investigated since the first half of the twentieth century (Salomon, 1929; Domaradzki, 1951). Early photogrammetrical and geodetic investigations gave surface displacements of several decimetres per year (Barsch and

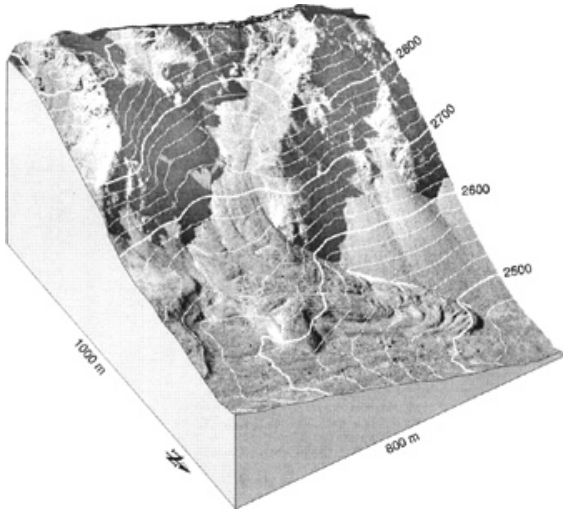

Figure 1 Synthetic oblique view of the Muragl rock glacier. A 1994 orthophoto and 20 m contour lines are draped over a perspective view of a 1994 digital terrain model (DTM). (At the upper edge the image frame is visible.).

Hell, 1975). Studies in the 1980s involved mapping and modelling of permafrost distribution (Haeberli, 1992; Keller, 1992; Hoelzle *et al*., 1993). Various geophysical soundings (Barsch, 1973; Vonder Mühll, 1993) gave an active layer thickness of about 2–7 m, and up to 20 m behind the front. Depths to bedrock increase from 50 m in the upper part to, presumably, 100 m and more in the lower part. At present, detailed geophysical soundings (Lehmann *et al*., 1998; Musil *et al*., 1999) and borehole monitoring (Arenson *et al*., 2000) are under way. Ongoing geodetic monitoring yields strong seasonal variations of surface velocities. Maximum speeds of up to 1 m a^{-1} are reached in (late) autumn, minimum speeds of only a few 0.01 m a^{-1} are found in spring and early summer at the same locations.

High-precision aerial photography (image scale approx. 1:6000) was started in 1981 and repeated in 1985, 1990, 1994, 1998 and 1999. The photoflights are performed by the Swiss Federal Office of Cadastral Surveys. First photogrammetric analysis (Vonder Mühll and Schmid, 1993) was repeated and extended using a technique of analytical photogrammetry (Kääb, 1996; Kääb *et al.* 1997; Kääb and Funk, 1999). Digital terrain models (DTMs) for 1981, 1985, 1990 and 1994, as well as horizontal surface velocities for the periods 1981–85, 1985–90 and 1990–94, all having 10 m grid spacing (approx. 2000 points), were obtained by Kääb (1998). By comparison with geodetic field measurements (Kääb, 1996; Kääb *et al*., 1997), a horizontal and vertical absolute accuracy of approx. ±0.2 m was estimated for individual heights and velocity vectors, respectively.

Figure 2 gives the average changes in elevation between 1981 and 1994 derived as differences of DTMs. The results show elevation changes within the range of ±0.1 m a^{-1}. Except for zones with perennial ice patches in the upper part of the creeping permafrost, where surface lowering of up to −0.5 m a^{-1} indicates massive loss of ice, the observed pattern of elevation changes is predominantly influenced by mass advection, especially at the fronts of individual lobes. Over the period investigated, the frozen debris of Muragl rock glacier was creeping with annual average surface speeds of up to 0.5 m a^{-1} (Figure 3). Maximum creep rates occur in the steeper middle part of the creeping permafrost. The flow field reveals the rock glacier to be a complex system of several flow lobes.

In order to evaluate the quality and accuracy of the new, fully digital techniques described in the next section, the above photogrammetric compilations were digitally repeated for the years 1981

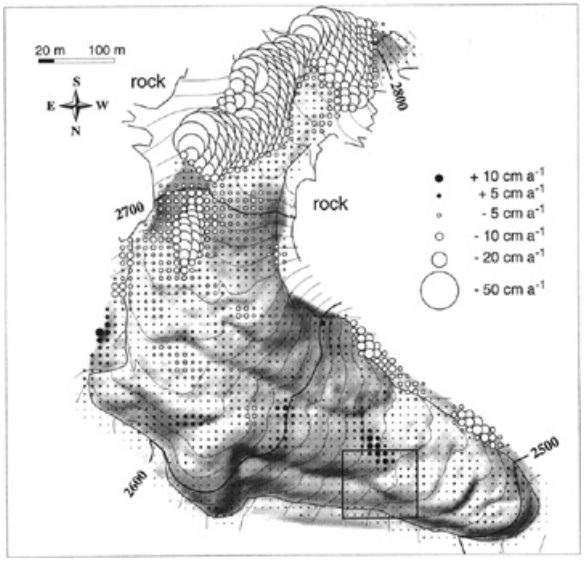

Figure 2 Average annual changes in surface elevation 1981–1994 as derived from analytical stereo-photogrammetry. Moderate permafrost heave and subsidence in the range of ±0.1 m a^{-1} in the lower part may indicate the sum of changes in ice content, three-dimensional straining and mass advection. Drastic lowering of up to −0.5 m a^{-1} in the upper part is due to pronounced melting of perennial ice patches. The rectangle to the lower right marks a region where detailed digital high-resolution measurements were performed (see Figure 10).

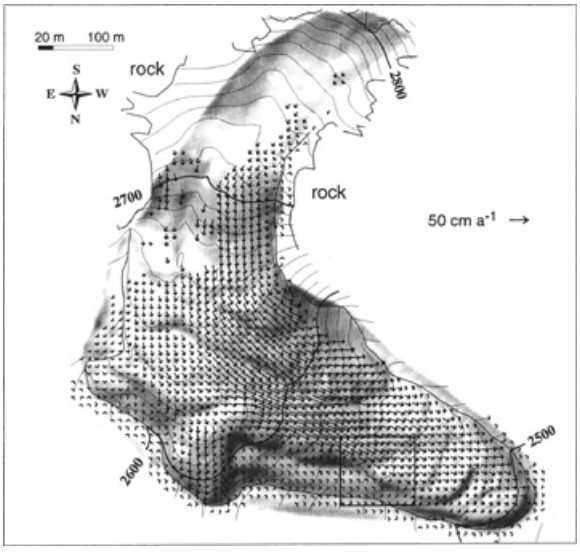

Figure 3 Average annual surface velocities between 1981 and 1994 as derived from multi-temporal image comparison using analytical stereo-photogrammetry. The velocity field with speeds of up to 0.5 m a^{-1} points to a complex system of individual lobes separated laterally as well as vertically. For the rectangle to the lower right see Figures 2 and 10.

and 1994 and compared with the above described reference results. Whilst these methods of analytical photogrammetry use analogue photographs (photographic films), the new digital techniques require digital imagery. The 1981 and 1994 photographs (black and white, 80% overlap) were scanned with 800 dpi ($\approx 30\,\mu$m in image units; ≈ 0.2 m in ground units) using a conventional low-cost scanner.

DIGITAL PHOTOGRAMMETRIC METHODS

Digital Terrain Models and Orthophotos

From overlapping digital images, DTMs with 10 m spacing and orthophotos with 0.2 m ground sampling distance were automatically derived for 1981 and 1994 using the commercial photogrammetric software SOCET SET (LH Systems, San Diego, California, USA). Figure 1 shows the 1994 orthophoto and contour lines draped over the 1994 DTM. As a special measure to improve the relative accuracy between the 1981 and 1994 images and their derived products, both image sets have been oriented and adjusted as one image segment. For this purpose, only stable terrain points (i.e. outside the rock glacier) have been used for ground control points and inter-annual image tie-points. The methodology of subsequent automatic DTM extraction and orthophoto generation from digital stereo imagery is well established and described (e.g. Grün and Baltsavias, 1987; Baltsavias *et al.*, 1996). The measurement of individual terrain heights is based on automatic assigning of corresponding terrain features in two (or more) overlapping images. For the final measurement the related correlation procedures focus on comparing image sections of only some pixels in size (in our case, 15 pixels or 3 m in ground units). Hence, heights can best be derived where, first, the optical contrast on the digital images is sufficient, e.g. not reduced due to fresh snow or surface grain sizes significantly lower than the image resolution, and, second, where terrain parts look similar on different photographs and are not strongly distorted or even occluded on the photographs, i.e. due to adjacent topography. Subsequently, the accuracy of the resulting DTM is generally reduced on steep slopes or in shadowy zones.

For the 1981 and 1994 orthophotos, the automatically extracted corresponding DTMs were used. As a basic characteristic of orthophoto generation, vertical errors in terrain elevation are transformed into horizontal deviations in pixel location. This effect is increasing towards the image margins. For the wide-angle camera used here (focal length 0.15 m) the ratio of height error to corresponding horizontal deviation ranges from 1 to 0 in the image centre to nearly 1 to 1 at the outermost image corners.

Surface Displacements

The horizontal surface displacements were derived from the 1981 and 1994 orthophotos of 0.2 m pixel size (ground units). Special photogrammetric software derives displacements of individual terrain features from multi-temporal digital orthophotos (CIAS correlation image analysis: Vollmer, 1999). Measuring an individual horizontal displacement vector basically follows two steps (Figure 4). First, in the orthophoto of time 1 (here 1981) an image section (so-called 'reference block') with sufficient optical contrast is chosen. The ground coordinates of its central pixel are known from the orthophoto geo-reference. Second, the corresponding image section (so-called 'test block') is searched for in a sub-area (so-called 'test area') of the orthophoto of time 2 (here 1994). If successfully found, the differences in central pixel coordinates directly give the horizontal displacement between time 1 and time 2 (Figure 4).

For identifying corresponding image blocks in both (or more) images, a double cross-correlation function based on grey values of the images is used:

$$\Phi(i,k) = \frac{\sum_j \sum_l s\left[(i+j,k+l) - \left(\frac{T_{\text{test}}}{N_{\text{test}}}\right)\right] \times m\left[(j,l) - \left(\frac{T_{\text{ref}}}{N_{\text{ref}}}\right)\right]}{\sqrt{\left\{\sum_j \sum_l s^2\left[(i+j,k+l) - \left(\frac{T_{\text{test}}}{N_{\text{test}}}\right)\right] \times \sum_j \sum_l m^2\left[(j,l) - \left(\frac{T_{\text{ref}}}{N_{\text{ref}}}\right)\right]\right\}}} \quad (1)$$

where Φ is the double cross-correlation function, (i, k) and (j, l) are the coordinates inside the test and reference blocks, s is the spatial grey-value function of the test block, $s(i, k)$ is the corresponding

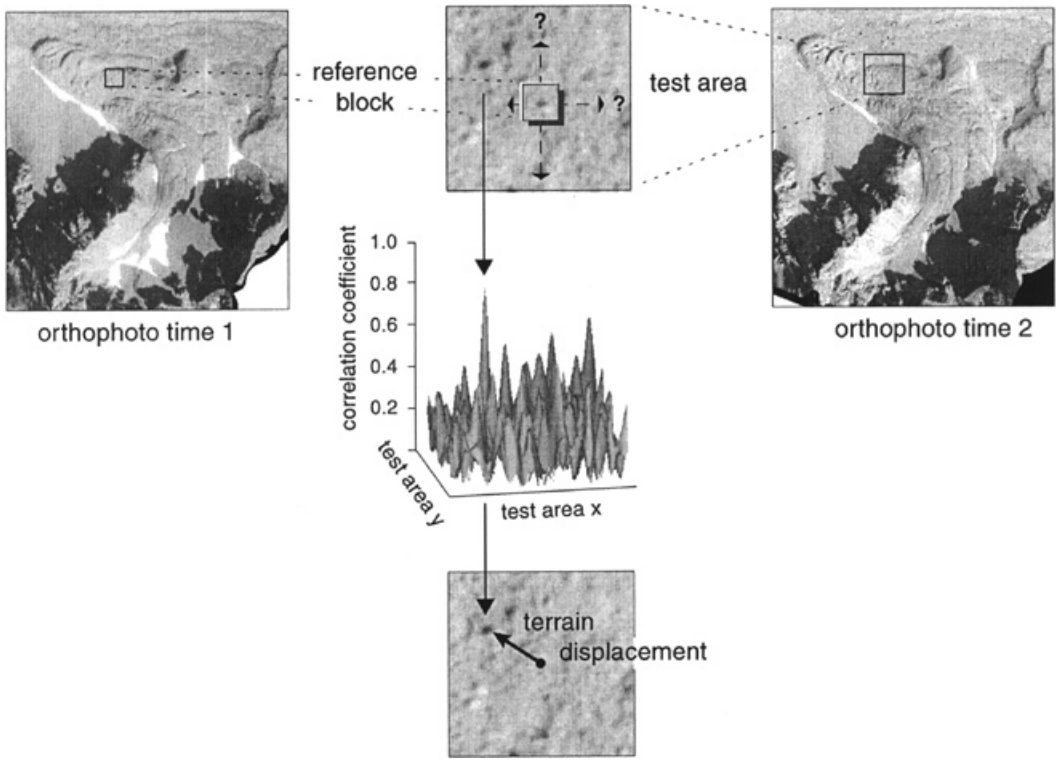

Figure 4 Schema of measuring surface displacements from repeated digital orthophotos by block-correlation techniques. A reference block in the orthophoto at time 1 is searched for in a test area in the orthophoto at time 2. The horizontal shift between the reference-block location and corresponding test block gives the surface displacement.

grey value at location (i, k), m is the spatial grey-value function of the reference block, $m(j, l)$ is the corresponding grey value at location (j, l), T is the sum of grey values of the test or reference block, and N is the number of pixels of the test or reference block ($N_{\text{ref}} = N_{\text{test}}$). The global maximum of Φ is taken to indicate the displaced terrain block of time 1. The T/N terms in equation (1) normalize the grey values of the test and reference blocks and ensure that differences in overall grey value do not affect the correlation result.

The size of the test area has to be chosen according to the expected maximum displacement, so that the test block which corresponds with the reference block can, in fact, be found in the test area. The size of the reference and test blocks has to be chosen according to the textural characteristics of the ground surface, i.e. the rock-glacier surface. If the block sizes are too small, Φ has no clear maximum; if the block sizes are too large, computing time soars drastically. Typical image-block sizes in our study range from 10×10 pixels to 30×30 pixels. Figure 5 indicates the influence of block size on the Φ-surface and the subsequent characteristics of global and regional maxima of Φ.

RESULTS AND QUALITY EVALUATION

Elevation Data

Operator-measured DTMs, like the reference DTM of 1994 used in this study, are characterized by high reliability of individual elevation values. Figure 6 shows the vertical differences between the operator-measured 1994 DTM and the raw results obtained by automatic DTM extraction from digital imagery. While the reference data have been measured from one stereo pair of photographs (60% overlap), the digital DTM generation was performed in three different ways: (1) based on two overlapping images of the rock glacier with 60% overlap, (2) based on two overlapping images with 80% overlap, and (3) using three overlapping images (80% overlap; see Figure 6).

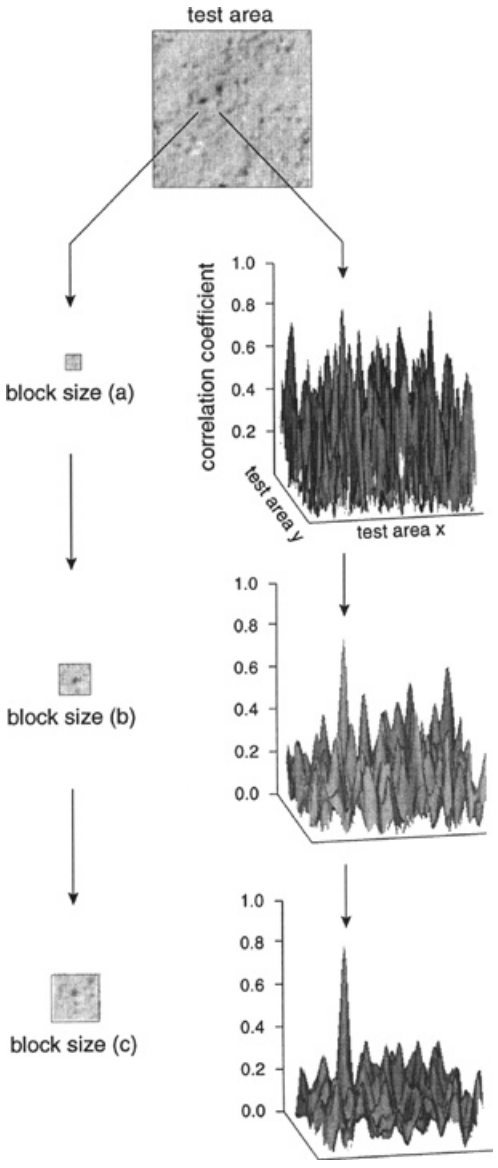

Figure 5 Influence of sizes of reference blocks on the surface Φ of correlation coefficients. The overall maximum of Φ indicates the most likely terrain displacement. Whereas small block sizes (e.g. (a) 10 × 10 pixels) often give no clear maximum, large block sizes (e.g. (c) 30 × 30) require long computing time. The optimal block size (e.g. (b) 20 × 20) has to be adapted to image resolution and optical terrain contrast.

For case 1 the differences between the reference and the digitally-derived DTM have a standard deviation of ±3.5 m and range from −35 m to +10 m. For case 2 the differences have a standard deviation of ±1.7 m and range from −11 m to +11 m. For case 3 the standard deviation is ±1.4 m and the range −16 m to +9 m. The different accuracies of cases 1 and 2, both using two images but with 60% and 80% overlap, are not surprising bearing in mind that the projective distortions strongly increase with decreasing overlap, which makes the automatic matching less successful. Where there is rough topography and steep terrain this influence outweighs the fact that 60% overlap gives a better geometry than 80%, and thereby a potentially better height determination.

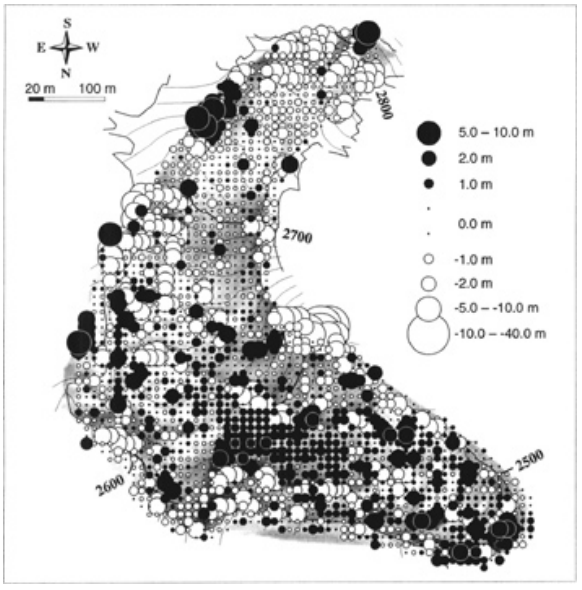

Figure 6 Raw differences between the 1994 reference DTM (operator-measured using analytical stereo-photogrammetry) and the 1994 DTM automatically derived from digital imagery (digital photogrammetry). Largest deviations occur on steep, shadowy, snowy, narrow or rough terrain parts. For better visibility, selected positive deviations (black circles) are highlighted by white borders. Note that maximum differences are not depicted on a linear scale.

Case 3, where three images with 80% overlap were used, seems comparable to case 2. Analysing case 3 in more detail (Figure 6) clearly shows that the large differences are mainly found in areas with less favourable terrain conditions, i.e. steep slopes, rough topography, low optical contrast or snow patches. Under favourable conditions, for instance on the rock-glacier lobes, the standard deviation amounts to approximately ±0.6 m and the maximum DTM differences lie in the range of approximately ±1.5 m. At this point we stress that the complex parameters specifying the automatic photogrammetric DTM extraction (i.e. the number of iterations, correlation window size, strategies etc.) have a significant influence on high-precision measurements. In this study we chose the default values of the software.

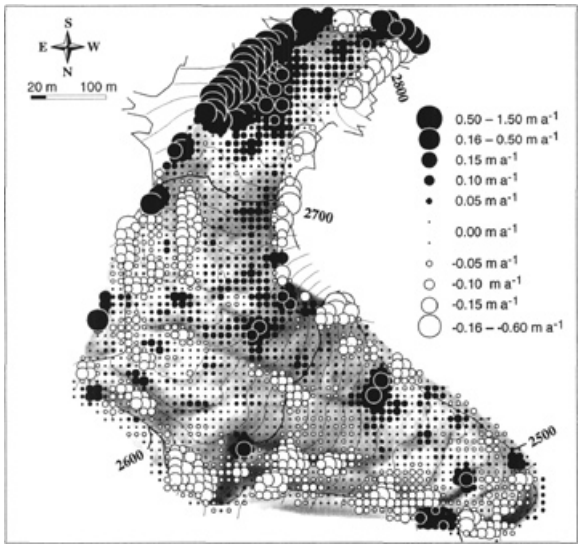

Figure 7 Differences between the elevation changes 1981–1994 deduced from operator-measured DTMs (see Figure 2) and the elevation changes 1981–1994 deduced from digitally-extracted DTMs. Both data sets have been smoothed using a 3 × 3 cell Gaussian low-pass filter. For better visibility, selected positive deviations (black circles) are highlighted by white borders. Note that maximum differences are not depicted on a linear scale.

As for the reference data (Figure 2), the elevation differences between 1981 and 1994 were also calculated from the automatically extracted DTMs of 1981 and 1994. A 3 × 3 cell, low-pass filter was applied to the raw DTM differences. Thereby, a new elevation difference was deduced as a weighted average value from the eight surrounding and the central elevation changes (Kääb *et al.*, 1997; Kääb and Funk, 1999). Elevation changes smoothed in such a way probably represent local changes in permafrost thickness rather than high-frequency point-by-point changes. In fact, for most applications concerning rock-glacier monitoring, the elimination of high-frequency components of elevation changes, which are strongly influenced by measurement noise, is appropriate. Therefore, the reference elevation changes (Figure 2) are given as low-pass filtered data. Figure 7 shows the differences between the operator-measured thickness changes (Figure 2) and the automatically-derived ones. The absolute differences between the two data sets amount to 0.06 m a^{-1} on average, with a standard deviation of ±0.13 m a^{-1}. Maximum errors of 1 m a^{-1} and more can be detected at the rock walls. Under favourable conditions, e.g. on the lobes, the differences decrease to 0.03 m a^{-1} on average, with a standard deviation of ±0.02 m a^{-1}. From Figures 6 and 7 the accuracy zones of the automatic DTM extraction can easily be distinguished. Elevation accuracy obviously reduces with both increasing frequency and amplitude of surface topography.

The operator-measured reference DTMs used in this study are not free of error. The average error of the reference DTM was estimated to be ±0.2 m. Thus, a majority of the differences with the reference elevation data are not significant. In summary, the error of the automatically-extracted DTM affects (1) the calculation of thickness changes from repeated DTMs, and (2) the horizontal pixel locations of the orthophotos which are used for automatic displacement measurements.

Velocity Field

Two different analyses were performed to evaluate the quality of horizontal displacement vectors measured by the orthophoto correlation: (1) displacements were measured from two orthophotos, both from 1994 and both computed using the same automatically-derived DTM, but both derived from two different original images; (2) surface displacements on the Muragl rock glacier between 1981 and 1994 were digitally measured using CIAS and then compared with the reference velocity field derived by an analytic plotter. For both test procedures a 10 m grid over the lower part of the rock glacier was measured. For each individual measuring point a test-area size of 100 × 100 pixels (20 × 20 m) and a reference/test-block size of 20 × 20 pixels (4 × 4 m) was chosen (see Figure 5).

TEST 1.

In the first test, two different orthophotos of 1994 were compared. Both orthophotos were generated using the identical automatically-extracted DTM of 1994, but were derived from two different original images, i.e. the leftmost and the rightmost image of the three 1994 photos (60% overlap). Basically, one would expect that the related CIAS analysis yields zero displacement for each of the 1600 points, because both images were taken at the same time (i.e. no rock-glacier motion). However, two potential influences could cause error in geometry and radiometry.

First, deviations of the DTM from the real terrain height lead to horizontal shifts of individual orthophoto pixels. Such dislocations have different directions on orthophotos generated from different original images. Each dislocation vector is radial to the respective image centre, and the resulting

shift between corresponding orthophoto pixels is coplanar with the so-called epipolar plane spanned by two projection centres and the projected terrain point (Baltsavias, 1996; Ladstädter, 1999). As a consequence, errors in the basic DTM finally lead to apparent displacements overlying the real displacements caused by permafrost deformation.

Second, the depicted terrain looks different in terms of radiometry in images taken from different places, and likewise in the orthophotos generated from these different images. Such image differences potentially reduce the correlation accuracy and may even lead to mismatches.

Figure 8 shows the vectors obtained from displacement measurements from two different 1994 orthophotos. The deviations from the expected zero displacement are on average 0.29 m ± 0.49 m. Corresponding amounts are obtained for the deviation direction. If measurements with $\Phi < 0.6$ are filtered out, approximately 1560 points (i.e. *c*. 97% of the original 1600) remain with an average deviation of 0.24 m ± 0.26 m; if measurements with $\Phi < 0.8$ are filtered out, around 1200 points (i.e. *c*. 75% of the original 1600: Figure 8) remain with an average deviation of 0.21 m ± 0.20 m. The latter deviation value equals the orthophoto pixel size (0.2 m). Maximum deviations are as great as 1.8 m. As expected, the largest errors occur on strongly undulated terrain, sharp edges, steep slopes, ditches, snow-covered terrain, shadow zones etc. Additionally, the displacement-error pattern shows significant agreement with the pattern of errors in the DTM used (cf. Figures 6 and 7) which points to the projection of DTM errors into planimetric errors in the orthophotos.

TEST 2.

As a second test, the displacements between 1981 and 1994 were derived with CIAS from 1981 and 1994 orthophotos, both generated from automatically extracted DTMs. The results were compared with the reference data which are operator-measured on an analytical plotter (see Figure 3). The filtering of the 1100 original measurements of test 2 resulted in 850 remaining points with $\Phi > 0.8$. This number represents *c*. 75%, which is similar to the result for the 1994–1994 test (also 75% remaining): this points primarily to the good conservation of the rock-glacier surface over 13 years. Obviously, the debris surface was not, or only little, affected by local activity except general creep and heave/settlement. The average difference in speed between the reference velocity field and the digitally-derived one is $0.02\,\mathrm{m\,a^{-1}} \pm 0.03\,\mathrm{m\,a^{-1}}$ i.e. not significant (Figure 9). Analogous amounts are obtained for the deviation direction. In the steep part of the rock glacier, at around 2550 m ASL, the error vectors show a more or less uniform direction, a fact that hints to a systematic error either in the reference or in the automatically-derived data. Error sources could be DTM errors, distortions in the relative image orientation, or faulty terrain interpretation.

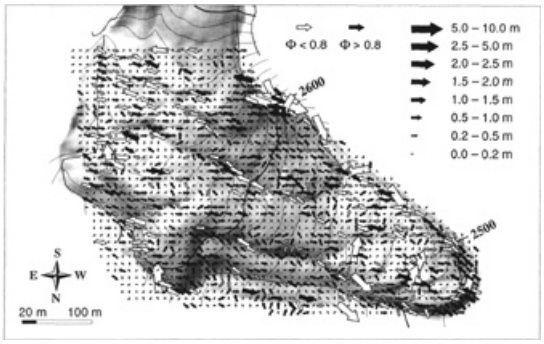

Figure 8 Displacement vectors as automatically measured from comparison of two digital orthophotos of the same date in 1994 but different camera locations. Thus, zero deviations would be expected. Because the two orthophotos have been generated from the same automatically-derived DTM but from different (overlapping) images, the actually obtained 'apparent displacements' are due to errors in the used DTM and due to mismatches caused by difficult terrain conditions. Black arrows indicate measurements with a correlation value better than 0.8. Measurements with correlation values worse than 0.8 (white arrows) would normally be eliminated automatically.

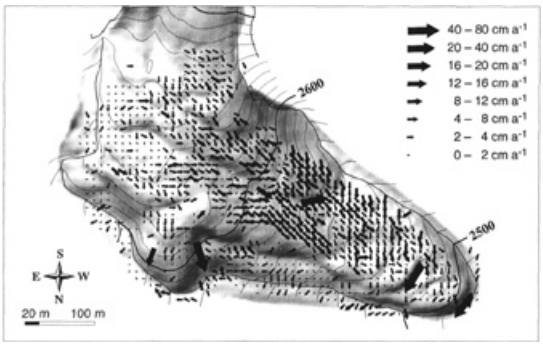

Figure 9 Differences between the operator-derived and the digitally-derived surface displacements for 1981–1994. On average, the deviations amount to approximately 10% of total speed. Bearing in mind the accuracy of the reference velocity vectors (approx. $\pm 0.02\,\mathrm{m\,a^{-1}}$) the obtained deviations are mostly not significant. Note that the depicted arrows indicate a two-dimensional error vector but not any kind of surface displacements.

With respect to the average speed of 0.2 m a^{-1}, the results represent an error of about 10%. Therefore, the digitally-derived displacements have at least a similar accuracy as the reference data (estimated error *c*. 10–15%).

VERY HIGH-RESOLUTION MEASUREMENTS

The main potential of automatic digital image analysis is its high speed of data acquisition. This allows for point resolutions which cannot be achieved with reasonable expenditure using conventional techniques. As an example, we present the 2.5 m spaced thickness changes and 3 m spaced displacements of a section of the Muragl rock glacier around the recently drilled boreholes mentioned in the introduction (Figure 10). The thickness changes have been Gaussian low-pass filtered. Displacements have been measured with test-block sizes of 15 × 15 pixels (3 m in ground units) and vectors with $\Phi < 0.8$ have been deleted. Comparison of the very high-resolution data with the conventional results (insets in Figures 2 and 3) clearly shows the wealth of detail which can be obtained from digital image analysis.

Between 1981 and 1994 distinct zones of settlement and heaving can be identified (Figure 10 left). Settlement could be due to erosion at steep flanks (e.g. at 2530 m ASL) or, indeed, to a decrease of ice content. The marked heaving to the south (*c*. 2550 m ASL) represents the sum of two different processes: a general heaving of roughly 0.06 m a^{-1} is overlain by the advection of the ridges. The displacement of the micro-topography can be seen from the coincidence between the high-frequency pattern of elevation changes and the surface topography (cf. Kääb *et al*., 1998). It can, furthermore, be derived that the micro-topography is advected downstream with a speed slightly lower than that of the permafrost creep (cf. Figure 10 right). These measurements and similar results on Murtél rock glacier (Kääb *et al*., 1998) suggest that the typical ridge-and-furrow topography of many rock glaciers, in fact, represents the deformation history of the frozen body in a cumulative way. However, advection of micro-topography alone would result in a balance of heaving in front of the advected ridges and of equivalent lowering at their rear. The difference to the observed pattern in elevation changes is the above-mentioned general heave overlying the displacement of the micro-topography. This low-frequency heave could be an expression of compressive flow and subsequent vertical extension at the creep lobe (see below for further discussion of the three-dimensional straining).

The measured surface displacements depict a drastic lateral shearing between the highly active part of the rock glacier and the low or even inactive part to the north-eastern margin (cf. Frauenfelder and Kääb, 2000). In fact, during drilling borehole 1,

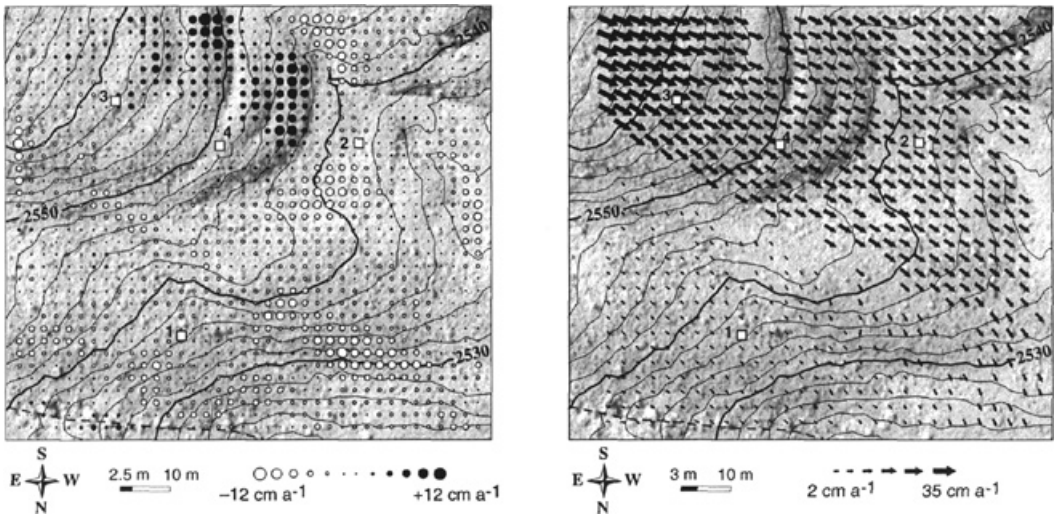

Figure 10 Permafrost thickness changes with 2.5 m spacing (left) and 3 m spaced horizontal displacements (right) automatically measured for a section of the Muragl rock glacier between 1981 and 1994 (see insets in Figures 2 and 3). The small rectangles indicate the location of boreholes 1–4 recently drilled by the Federal Institute of Technology, Switzerland. The dashed line to the north represents the margin of the rock glacier. Underlying orthophoto of 1994.

no ice was found, whereas at boreholes 2–4 a low ice content of the matrix was detected (Arenson *et al*., 2000). Together with the general topography, the sharp speed gradients clearly show an active lobe overriding one or several inactive layers. Disagreement of today's velocity field with the actual surface topography of the creeping permafrost thus points to changed internal or external conditions of rock-glacier development.

Longitudinal surface deformation in the highly active part, where surface speeds decrease from $35\,\mathrm{cm\,a^{-1}}$ to *c*. $18\,\mathrm{cm\,a^{-1}}$ within a few decametres, reaches values of up to $0.003\,\mathrm{a^{-1}}$. Hypothetically, assuming incompressible material and a linear variation of strain rates with depth, the measured compression would correspond to 1–2 centimetres of surface heave per year and per 10 m thickness of the deforming layer. Bearing in mind the low ice content found in the boreholes, the incompressibility assumption is certainly critical. Therefore, the surface heave calculated by three-dimensional straining expresses a qualitative estimation of mass accumulation by compressive creep.

However, the (not depicted) horizontal strain rates, derived as spatial gradients of the flow field (Kääb *et al*., 1997; Kääb, 1998), show both a significant spatial correlation with the observed pattern of elevation changes and the occurrences of transverse ridges and furrows. Thus, the spatial flow-field derivatives indicate, first, the significant influence of three-dimensional straining on the temporal development of surface geometry and, second, a connection between compressive flow and transverse ridge-and-furrow topography (cf. Kääb *et al*., 1997; 1998).

A further result of the measured high-resolution displacements (Figure 10 right)—which are displayed raw and unsmoothed, in contrast to the smoothed elevation changes (Figure 10 left)—is the uniformity of the surface deformation. Besides strong lateral shearing, no spatial high-frequency variations can be seen in the velocity field. The mass is obviously deforming as a whole with some stress transferring material components (ice). Therefore, the observed movements are not the sum of individual displacements of debris components.

CONCLUSIONS AND PERSPECTIVES

Digital photogrammetric techniques are highly efficient when determining geometry, geometry changes and surface flow of permafrost creep phenomena. Accuracy is at least similar to that achieved by conventional photogrammetric techniques. The reliability of individual, automatically measured surface elevations or displacements is significantly lower than operator-measured ones. For rock glaciers, inaccurate or outlying measurements occur because of rough micro-topography, snow coverage, steep slopes and where optical terrain contrast falls below the image resolution. In order to eliminate such error, operator control by stereo vision and related editing of an automatically-derived DTM is essential for deriving high-quality DTMs and detecting small changes in permafrost creep.

Digital image analysis allows for much higher data acquisition speed and data resolution than conventional techniques. The possibility of deriving thickness changes, velocity fields and deformation fields for large areas, often covering entire rock glaciers or even entire regions, opens new perspectives for understanding permafrost creep in space and time. Furthermore, high-resolution applications promote new insights into the processes of permafrost creep, such as the development of micro-topography, rock-glacier advance mechanisms, and other mass-movement processes. Digital image analysis could be improved by advanced image pre-processing (e.g. Förstner and Gülich, 1987), knowledge-based result post-processing, and enhanced block-matching techniques and multi-image approaches (e.g. Grün and Baltsavias, 1987; Ladstädter, 1999). Digital data flow will be improved by airborne high-resolution digital imaging sensors (e.g. HRSC: Hauber *et al*., 2000) and high-resolution satellite imagery.

ACKNOWLEDGEMENTS

We gratefully acknowledge the careful and constructive comments of two referees. Thanks are due to Regula Frauenfelder and Martin Hoelzle for their valuable discussions on the manuscript, and to Wilfried Haeberli for his continuous support of the work. We also want to thank Rolf Hübscher, Hans-Peter Gautschi and Daniel Lüscher (Federal Office of Cadastral Surveys) for acquisition of the aerial photographs. Philippe Meuret and Bruno Weber set up and helped run the digital photogrammetric station.

REFERENCES

Arenson L, Vonder Mühll D, Springman S. 2000. Drilling in the Muragl rock glacier. Abstract. In *Geophysical Research Abstracts, European Geophysical Society. 25th General Assembly, Nice, France*.

Baltsavias EP. 1996. Digital ortho-images – a powerful tool for the extraction of spatial- and geo-information. *ISPRS Journal of Photogrammetry and Remote Sensing* **51**(2): 63–77.

Baltsavias EP, Li H, Stefanidis A, Sinning M. 1996. Automatic DSMs by digital photogrammetry. *Surveying World* **4**(2): 18–21.

Barsch D. 1973. Refraktionsseismische Bestimmungen der Obergrenze des gefrorenen Schuttkörpers in verschiedenen Blockgletschern Graubündens. *Zeitschrift für Gletscherkunde und Glazialgeologie* **9**(1–2): 143–167.

Barsch D, Hell G. 1975. Photogrammetrische Bewegungsmessung am Blockgletscher Murtèl I, Oberengadin, Schweizer Alpen. *Zeitschrift für Gletscherkunde und Glazialgeologie* **11**(2): 111–142.

Berthling I, Etzelmüller B, Eiken T, Sollid JL. 1998. Rock glaciers on Prins Karls Forland, Svalbard. I: Internal structure, flow velocity and morphology. *Permafrost and Periglacial Processes* **9**: 135–145.

Domaradzki J. 1951. Blockströme im Kanton Graubünden. Ergebnisse der wissenschaftlichen Untersuchung des schweizerischen Nationalparks. *Kommission der Schweizerischen Naturforschenden Gesellschaft*, III/24, 177–235.

Förstner W, Gülich E. 1987. A fast operator for detection and precise location of distinct points, corners and centers of circular features. In *Proceedings of Fast Processing of Photogrammtric Data, Interlaken, Switzerland*, 281–305.

Frauenfelder R, Kääb A. 2000. Towards a palaeoclimatic model of rock glacier formation in the Swiss Alps. *Annals of Glaciology* **31**, in press.

Gorbunov AP, Titkov SN. 1992. Dynamics of rock glaciers of the northern Tien Shan and the Djungar Ala Tau, Kazakhstan. *Permafrost and Periglacial Processes* **3**: 29–39.

Grün A, Baltsavias E. 1987. High precision image matching for digital terrain model generation. *Photogrammetria* **42**: 97–112.

Haeberli W. 1992. Possible effects of climate change on the evolution of Alpine permafrost. *Catena Supplement* **22**: 23–35.

Haeberli W, Schmid W. 1988. Aerophotogrammetrical monitoring of rock glaciers. In *Proceedings of the 5th International Conference on Permafrost*; Trondheim Norway, Vol. 1, 764–769.

Haeberli W, King L, Flotron A. 1979. Surface movement and lichen-cover studies at the active rock glacier near the Grubengletscher, Wallis, Swiss Alps. *Arctic and Alpine Research* **11**(4): 421–441.

Haeberli W, Hoelzle M, Kääb A, Keller F, Vonder Mühll D, Wagner S. 1998. Ten years after drilling through the permafrost of the active rock glacier Murtèl, Eastern Swiss Alps: answered questions and new perspectives. In *Proceedings of 7th International Permafrost Conference, Yellowknife*; Nordicana 57, 403–410.

Haeberli W, Kääb A, Wagner S, Geissler P, Haas JN, Glatzel-Mattheier H, Wagenbach D, Vonder Mühll D. 1999. Pollen analysis and ^{14}C-age of moss remains recovered from a permafrost core of the active rock glacier Murtèl/Corvatsch (Swiss Alps): geomorphological and glaciological implications. *Journal of Glaciology* **45**(149): 1–8.

Hauber E, Slupetzky H, Jaumann R, Wewel F, Gwinner K, Neukum G. 2000. Digital and automated high resolution stereo mapping of the Sonnblick glacier (Austria) with HRSC-A. In *Proceedings of the EARSL Workshop, Dresden, Germany*, in press.

Hoelzle M, Haeberli W, Keller F. 1993. Application of BTS-measurements for modelling permafrost distribution in the Swiss Alps. In *Proceedings of 6th International Conference on Permafrost, Beijing, China*; Nordicana 57, Vol. 1, 272–277.

Hoelzle M, Wagner S, Kääb A, Vonder Mühll D. 1998. Surface movement and internal deformation of ice-rock mixtures within rock glaciers in the Upper Engadin, Switzerland. In *Proceedings of 7th International Conference on Permafrost, Yellowknife, Canada*; Nordicana 57, 465–472.

Kääb A. 1996. *Photogrammetrische Analyse zur Früherkennung gletscher- und permafrostbedingter Naturgefahren im Hochgebirge*. Mitteilungen der Versuchsanstalt für Wasserbau, Hydrologie und Glaziologie der ETH Zürich no. 145.

Kääb A. 1998. Oberflächenkinematik ausgewählter Blockgletscher des Oberengadins. In *Beiträge aus der Gebirgs-Geomorphologie. Jahrestagung 1997 der Schweizerischen Geomorphologischen Gesellschaft*. Mitteilungen der Versuchsanstalt für Wasserbau, Hydrologie und Glaziologie der ETH Zürich no. 158, 121–140.

Kääb A, Funk M. 1999. Modelling mass balance using photogrammetric and geophysical data. A pilot study at Gries glacier, Swiss Alps. *Journal of Glaciology* **45**(151): 575–583.

Kääb A, Haeberli W, Gudmundsson GH. 1997. Analyzing the creep of mountain permafrost using high precision aerial photogrammetry: 25 years of monitoring Gruben rock glacier, Swiss Alps. *Permafrost and Periglacial Processes* **8**: 409–426.

Kääb A, Gudmundsson GH, Hoelzle M. 1998. Surface deformation of creeping mountain permafrost. Photogrammetric investigations on rock glacier Murtèl, Swiss Alps. In *Proceedings of the 7th International Permafrost Conference, Yellowknife, Canada*; Nordicana 57, 531–537.

Kaufmann V. 1998. Deformation analysis of the Doesen rock glacier (Austria). In *Proceedings of the 7th International Permafrost Conference, Yellowknife, Canada*; Nordicana 57, 551–556.

Keller F. 1992. Automated mapping of mountain permafrost using the program PERMAKART within the geographical information system ARC/INFO. *Permafrost and Periglacial Processes* **3**(2): 133–138.

Konrad SK, Humphrey NF, Steig EJ, Clark DH, Potter N Jr, Pfeffer WT. 1999. Rock glacier dynamics and paleoclimatic implications. *Geology* **27**(12): 1131–1134.

Krummenacher B, Budmiger K, Mihajlovic D, Blank B. 1998. *Periglaziale Prozesse und Formen im Furggentälti, Gemmipass*. Mitteilungen des Eidgenössisches Institutes für Schnee- und Lawinenforschung no. 56.

Ladstädter R. 1999. Automatisierte Messung von Geländemodellen und Fliessvektoren aus digitalen, multitemporalen Orthophotos—ein neuer Ansatz für das Blockgletscher-Monitoring. Diploma thesis, Technical University of Graz, Austria.

Lehmann F, Vonder Mühll D, Van der Veen M, Wild P, Green A. 1998. True topographic 2-D migration of georadar data. In *Expanded Abstracts, 11th Annual Symposium on the Applications of Geophysics to Environmental and Engineering Problems (SAGEEP), Chicago, USA*; 107–114.

Messerli B, Zurbuchen M. 1968. Blockgletscher im Weissmies und Aletsch und ihre photogrammetrische Kartierung. *Die Alpen, SAC* **3**: 139–152.

Musil M, Maurer HR, Horstmeyer H, Nitsche FO, Vonder Mühll D. 1999. High-resolution seismic measurements on an Alpine rock glacier. In Expanded Abstracts, *5th Meeting of the Environmental and Engineering Geophysical Society, European Section, Budapest, Hungary*, in press.

Salomon W. 1929. *Arktische Bodenformen in den Alpen*. Sitzungsbericht der Heidelberger Akademie der Wissenschaften. Mathematisch-naturwissenschaftliche Klasse 5. Abhandlungen Walter de Gruyter, no. 31.

Vollmer M. 1999. Kriechender alpiner Permafrost: Digitale photogrammetrische Bewegungsmessung. Diploma thesis, Department of Geography, University of Zurich.

Vonder Mühll DS. 1993. *Geophysikalische Untersuchungen im Permafrost des Oberengadins*. Mitteilungen der Versuchsanstalt für Wasserbau, Hydrologie und Glaziologie der ETH Zürich, no. 122.

Vonder Mühll DS, Schmid W. 1993. Geophysical and photogrammetrical investigation of rock glacier Muragl I, Upper Engadin, Swiss Alps. In *Proceedings of the 6th International Conference on Permafrost, Beijing, China*; South China University of Technology, Vol. 1, 214–219.

